Journal of Innovative Optical Health Sciences
Vol. 2, No. 4 (2009) 423–430
© World Scientific Publishing Company

World Scientific
www.worldscientific.com

J. Innov. Opt. Health Sci. 2009.02:423-430. Downloaded from www.worldscientific.com
by HUAZHONG UNIVERSITY OF SCIENCE AND TECHNOLOGY on 10/24/18. Re-use and distribution is strictly not permitted, except for Open Access articles.

ASSESSING WORKING MEMORY IN REAL-LIFE SITUATIONS WITH FUNCTIONAL NEAR-INFRARED SPECTROSCOPY

TING LI, LI LI, QINGMING LUO and HUI GONG*
Britton Chance Center for Biomedical Photonics
National Laboratory for Optoelectronics
Huazhong University of Science and Technology
Wuhan 430074, P. R. China
**huigong@mail.hust.edu.cn*

Working memory is one of the most important functions in our brain, which has been widely studied with unreal-life measured technologies. A functional near-infrared spectroscopy (fNIRS) instrument with a portable and low-cost design is developed, which is capable of providing hemodynamic measurement associated with brain function in real-life situations. Using this instrument, we performed working memory studies involved in Chinese words encoding, verbal, and spatial stem recognition, which are mainly studied with other technologies. Our results show that fNIRS can well assess working memory activities, in comparison with the reported results mainly using other methodologies. Furthermore, we find that hemodynamic change in the prefrontal cortex during all working memory tasks is highly associated with subjects' behavioral data. fNIRS is shown to be a promising alternative to the current methodologies for studying or assessing functional brain activities in natural condition.

Keywords: Functional near-infrared spectroscopy (fNIRS); working memory; prefrontal cortex (PFC); oxy-hemoglobin; deoxy-hemoglobin.

1. Introduction

The capability of near-infrared spectroscopy (NIRS), to noninvasively measure the hemoglobin oxygenation changes in biological tissues, was first described by Jobsis in 1977.[1] NIRS has been originally designed for clinical monitoring, including muscle oximeters[2,3] and breast imaging.[4,5] Since the early 1990s, NIRS has been introduced as a useful tool for neuroimaging studies (functional near-infrared spectroscopy (fNIRS)).[6–8] fNIRS uses specific wavelengths of light, transporting through the scalp and cerebrospinal fluid, to measure the relative oxygenation change in the brain tissue during brain activities. This technology allows the instrument design to be portable, affordable, noninvasive, nonionizing, and safe. These features make fNIRS suitable to study the hemodynamic responses to cognitive activity in real-life situation, such as under working or educating.

Functional brain imaging is mainly conducted to understand the brain activity in a target brain region or the communication with other regions, as well as the pathway to the specified brain function. Up to now, the fNIRS researches on cognition have focused on its association with Brodman's areas BA9, BA10, BA46, BA45, BA47, and BA44

*Corresponding author.

J. Innov. Opt. Health Sci. 2009.02:423-430. Downloaded from www.worldscientific.com
by HUAZHONG UNIVERSITY OF SCIENCE AND TECHNOLOGY on 10/24/18. Re-use and distribution is strictly not permitted, except for Open Access articles.

(all in the frontal lobe).[9–13] These areas, as shown in measurements by functional magnetic resonance imaging (fMRI) and positron emission tomography (PET), play a crucial role in both short-term storage and executive process components of working memory.[14–16] Additionally, both the storage of verbal materials and the word recognition have also been reported to be correlated with the left hemisphere.[16,17] Some fNIRS measurements were consistent with fMRI and PET findings for n-back verbal working memory.[13]

Here we focus on the prefrontal cortex (PFC) in hemodynamic response to working memory which are mainly studied with PET, fMRI, and EEG, including Chinese word encoding, spatial, and verbal stem recognition. The involvement of PFC in working memory was not consistently observed. By measuring the PFC activation interpreted by hemodynamic changes with fNIRS, we expect to explore whether PFC involves in working memory and, if true, further explore the activation pattern in PFC under different types of working memory.

We will first introduce our fNIRS instrument. Then, the current results on working memory researches which were conducted in our lab are presented. Finally, the activation feature of PFC in hemodynamic to working memory is summarized and discussed, as well as the merits of optical imaging in assessing working memory.

2. Functional Near-Infrared Spectroscopy

2.1. *fNIRS instrument*

In the studies described throughout this paper, we used the portable CW-type fNIRS instrument developed in our lab.[18] CW-type instrument in which light is applied to tissue at constant amplitude is limited to measuring amplitude attenuation to the incident light. CW-type instrument is advantageous at low cost, portability, and easier to construct. This instrument contains four components as shown in Fig. 1: (1) The probe that can softly cover almost the whole forehead. The area of the probe is 4.4 cm × 15 cm. In usage, the probe is symmetrically covered from the eyebrow to the hairline on the forehead, which is commonly called PFC. (2) A data acquisition board. (3) A controller which drives the probe, controlling the work time sequence of the probe and the data acquisition. (4) A computer with a software to sample data and real-time display the data, as well as perform the offline data analysis. Its sampling rate is optional from 0.4 Hz to 4 Hz.

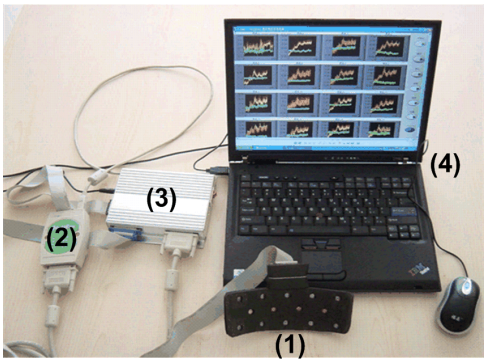

Fig. 1. A construction picture of fNIRS system.

As shown in Fig. 2, the flexible probe consists of four light sources, each one of which contains built-in LEDs having peak wavelengths at 735 and 850 nm, and ten detectors to image the hemodynamic changes in the PFC. Each fixed source–detector separation is 2.89 cm. The configuration of light sources and detectors allows 16 channels simultaneously in data sampling. The flexible probe consists of a flexible circuit board with LEDs and detectors welded on it, two thin pieces of man-made cushioning material are attached on each side of the circuit board. Since both of the circuit board and cushioning material are flexible and light (50 g), the probe can be moved randomly and adapt to the surface shape of subjects' foreheads and make

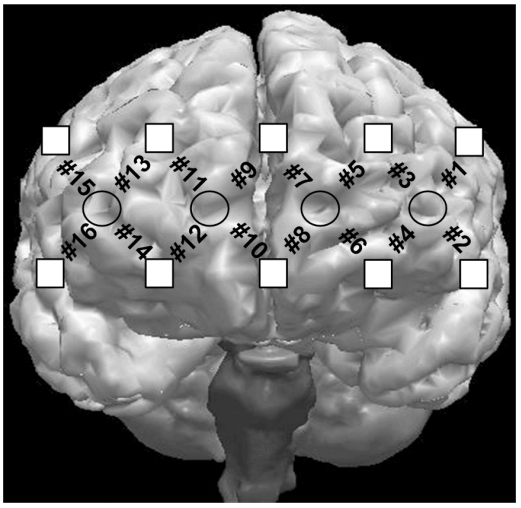

Fig. 2. Detecting areas of fNIRS in the prefrontal cortex. Circles denote light sources; panes denote detectors. "#1", "#2", . . . , and "#16" denote the detected channels.

J. Innov. Opt. Health Sci. 2009.02:423-430. Downloaded from www.worldscientific.com
by HUAZHONG UNIVERSITY OF SCIENCE AND TECHNOLOGY on 10/24/18. Re-use and distribution is strictly not permitted, except for Open Access articles.

subjects suitable, allowing to improve the light coupling efficiency, signal intensity, and the ratio of signal to noise.

The fNIRS instrument has been fully evaluated for its performance.[18] Especially, the noise equivalent power is smaller than 110 pw; the dynamic range gets to 62 dB; the baseline drift is smaller than 0.7%; the maximum exposure of light source is 0.03 W/cm^2; the detectable penetration depth is a maximum of about 2.5 cm from the scalp, which can make the light penetrate the scalp, skull, and cerebrospinal fluid; and detect cortical activity; the stray light rejection is lower than 1%. These qualities allow the fNIRS instrument to work effectively, stably and safely, as well as to sample high-quality signals.

2.2. *Measurement translation and signal processing*

fNIRS measures the light intensity using a photon detector. The hemodynamic signals are extracted from the raw fNIRS measurements with the modified Beer–Lambert law. The light attenuation of the incident light, which is due to both photons absorption and scattering, can be quantified as optical density (OD):

$$\mathrm{OD} = \log\left(\frac{I_0}{I}\right), \tag{1}$$

where I_0 and I represent the incident and emerged light intensities, respectively. During the functional brain activity, the scattering materials within different layers of the head make ignorable changes,[19] with a result that the scattering is considered to be constant. The light attenuation changes measured as a result of brain activity are due to the concentration variations of absorption materials in the brain tissue, called as oxygenated hemoglobin and deoxygenated hemoglobin (oxy-Hb, deoxy-Hb), which are related to the functional activity based on a widely accepted hypothesis called neurovascular coupling.[19]

According to the modified Beer–Lambert Law, the OD changes can be related with the variation in concentrations of oxy-Hb and deoxy-Hb (Δ[oxy-Hb], Δ[deoxy-Hb]).

$$\begin{aligned}\Delta\mathrm{OD}_{850} &= k\Delta[\text{oxy-Hb}] + k'\Delta[\text{deoxy-Hb}],\\ \Delta\mathrm{OD}_{735} &= t\Delta[\text{oxy-Hb}] + t'\Delta[\text{deoxy-Hb}].\end{aligned} \tag{2}$$

$\Delta\mathrm{OD}_{850}$ and $\Delta\mathrm{OD}_{735}$ denote OD changes at 850 and 735 nm, which are used in our instrument. With a blood–brain model experiment, ratios $k/t, k'/t'$, and t/t' can be valued by calculating the ratios of OD changes in fully-oxygenated and fully-deoxygenated states. The only remaining variant to determine all coefficients in Eq. (2) is dependent on the mean partial optical path length (PPF) within the activated brain area. However, measuring PPF is not feasible. Since PPF is actually dependent on the localization of activated brain area, variables Δ[oxy-Hb] and Δ[deoxy-Hb], here we integrate PPF into the variables Δ[oxy-Hb] and Δ[deoxy-Hb]. Hence, the scale of Δ[oxy-Hb] and Δ[deoxy-Hb] are mmol $\times$ mm and dependent on the path length of the near-infrared light in the head.[20] The final signal translation is given as

$$\begin{aligned}\Delta[\text{oxy-Hb}] &= \Delta\mathrm{OD}_{850} - 0.5643\Delta\mathrm{OD}_{735},\\ \Delta[\text{deoxy-Hb}] &= 0.7535\Delta\mathrm{OD}_{735} - 0.4341\Delta\mathrm{OD}_{850}.\end{aligned} \tag{3}$$

Here we use oxygenation to evaluate brain activation, which is equal to Δ[oxy-Hb] $-$ Δ[deoxy-Hb]. After measurement translation, we process signal offline analysis according to the following steps: (1) The singular signal, originated from the artifact of muscle movement or system error, is balanced with the nearest data using interpolation methods. (2) Different kinds of physiological noise, such as heart beat, pulse movement or breathing, are eliminated using principle component analysis. (3) The baseline is corrected by subtracting the data in the rest period; and the data are smoothed by window filtering of 5 point hamming. (4) The mean amplitude in the stable phase of oxygenation change for every channel/subject is also extracted for statistical analysis. (5) The bar plot or map of oxygenation changes are obtained with above amplitude values.

3. fNIRS Studies on Working Memory

In all the studies below, subjects have signed informed statements by the Human Subjects Institutional Review Board in the Huazhong University of Science and Technology. Different groups of three females and three males (age 22 ± 1.5 years, mean$\pm$SD, education degree 15.8 ± 1.2 years), every one of which is healthy, right-handed, and has normal or corrected-to-normal vision, take part in different experiments. During 24 h before experiment, none of the subjects had taken any tranquilizer or psychiatric drugs.

J. Innov. Opt. Health Sci. 2009.02:423-430. Downloaded from www.worldscientific.com
by HUAZHONG UNIVERSITY OF SCIENCE AND TECHNOLOGY on 10/24/18. Re-use and distribution is strictly not permitted, except for Open Access articles.

3.1. *Chinese word encoding: Comparison of structure cognition and semantic processing*

A block paradigm is employed referring to the relevant experiment paradigm on Chinese word semantic processing.[25,26] Considering that structure perception processing is one of crucial factors in semantic processing for the Chinese word encoding, this study makes both structure processing and semantic processing included in the paradigm and gets the measurement for targeted semantic encoding by subtracting that for structure processing.

The whole paradigm is shown in Fig. 3 and materials are 100 uncorrelated two-character words. These words are then composed to 50 pairs, 25 pairs for structure processing, and other 25 pairs for semantic processing. In structure processing, subjects are asked to orally justify if the characters of co-presented word pairs are both in same structure. The structures of Chinese characters are classified as two types: one is top to bottom; the other is left to right. In semantic processing, subjects are asked to group presented word pairs into a meaningful sentence. After the experiment, subjects are asked to report a value (range: 0–10; "10" denotes the difficulty score for unachievable tasks) to quantify task difficulty.

In the rest block of all experiments, a mark "+" is presented in the center of computer screen; each rest block is accompanied by a pure sound "ding" at 58 s as a test-coming hint; all stimulus and mark "+" are presented in white in contrast to the black background with font of Times New Roman and font size in 108. The distance between the 19 inch computer screen and subjects is set as about 110 cm to keep subjects' visual angles less than ±5° horizontally and vertically.

During the experiment, the PFC hemodynamic response is real-time collected. All subjects perform similar measurements; for example, the time sequence of fNIRS-measured hemodynamic response for subject 1 is shown in Fig. 4. In the figure, the rest phase is displayed with gray background; the first segment with white background denotes measurements for structure cognition; the second segment with white background denotes measurements for semantic processing. Figure 4 significantly shows that both Δ[oxy-Hb] and Δ[deoxy-Hb] in nearly all channels show a lower level activation during structure cognition and a higher level activation during semantic processing.

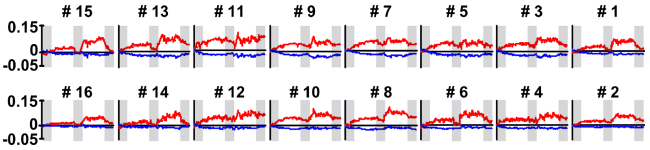

Fig. 4. Time courses of Δ[oxy-Hb] (red line) and Δ[deoxy-Hb] (blue line) obtained by fNIRS in some subject during the task of Chinese words encoding. Gray regions denote rest periods; the other regions denote the measurements for structure cognition and semantic processing in turn.

To further analyze the activation difference between structure cognition and semantic processing, we compare the PFC activation distribution of all subjects between the two tasks. All subjects show similar activation distribution in the same task. Here, we show the mean activation distribution interpreted by oxygenation across subjects, that is, Fig. 5. The pseudo-color maps in the figure are drawn with all of oxygenation values in detected channels by interpolation. Our previous studies on the same paradigm were performed with a four-channel fNIRS.[25,26] The result of those studies only reported a stronger response to semantic processing than structure cognition in the left PFC. In comparison, Fig. 5 shows not only the same polarity between the tasks in the left PFC activation amplitude, but also the opposite polarity in the middle

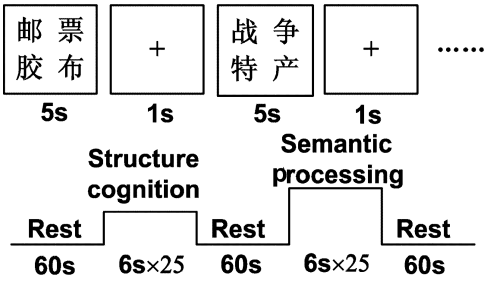

Fig. 3. Paradigm sketch of the Chinese words encoding experiment.

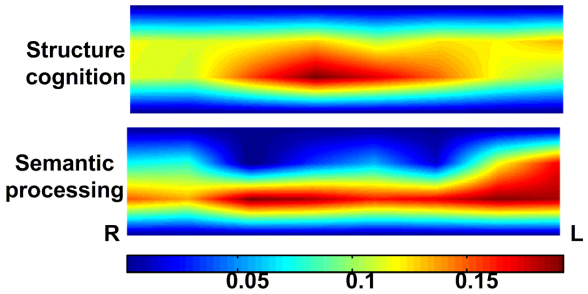

Fig. 5. Maps of oxygenation change for structure cognition and semantic process to Chinese words.

J. Innov. Opt. Health Sci. 2009.02:423-430. Downloaded from www.worldscientific.com
by HUAZHONG UNIVERSITY OF SCIENCE AND TECHNOLOGY on 10/24/18. Re-use and distribution is strictly not permitted, except for Open Access articles.

Table 1. Mean oxygenation changes (averaged over all channels) and oral reported difficulty scores for structure cognition and semantic processing to Chinese words.

Subject ID	ΔOxygenation structure	Difficulty score	ΔOxygenation semantic	Difficulty score
1	0.0600	7	0.0802	8
2	0.0426	5	0.0454	6
3	0.0083	2	0.0162	2
4	0.0390	5	0.0463	6
5	0.0281	3	0.0318	3
6	0.0489	6	0.0546	7

PFC. Our result fully shows that: (1) Structure cognition mainly activates the middle PFC, while the semantic processing mainly activates the left PFC. (2) Semantic processing invokes stronger in the left PFC, while the structure cognition invokes stronger and larger in the middle-to-left region of PFC.

We also compare the mean oxygenation across channels in relation to the self-feeling difficulty scores between the tasks. As shown in Table 1, for each subject, once the difficulty scores differ between tasks, the oxygenation changes are shown to be significantly different; the subjects whose difficulty score in semantic processing are higher than structure cognition also show higher mean oxygenation in semantic processing than structure cognition. There is a significant correlation between mean oxygenation change and self-feeling difficulty scores (difficulty score) for all subjects in PFC ($r = 0.958, p < 0.001$).

3.2. *Stem recognition: Comparison of verbal and spatial memory*

The experimental protocol mainly studied with PET is a complex paradigm composed of four test blocks, including verbal control, verbal memory, spatial control, and spatial memory.[21] There is a 1 min rest before and after each block. In verbal recognition, English letters are employed as stimuli. To make subjects not use shape but voice to code verbal materials, probing stimulus are set in lowercase and targeted stimulus are set in capital. In spatial recognition, black dots are used as targeted stimuli and circle is probing stimulus.

The paradigm of each task is shown in Fig. 6. During the experiment, subjects are asked to quickly and correctly respond by clicking the left mouse button to the matched cases and otherwise clicking the right mouse button. In both verbal control and verbal memory, the matched case is that there is a letter in the targeted stimulus whose lowercase letter is the same as the probing stimuli. In spatial recognition the matched case is that there is a circle looped around one dot presented 3 s before. Matched case is presented in a frequency of 50%.

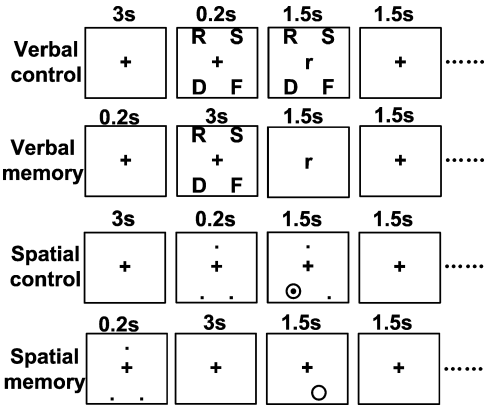

Fig. 6. Schematic paradigms of verbal control, verbal memory, spatial control, and spatial memory in stem recognition. The time value in each horizontal axis denotes presentation time for the stimulus shown in its below pane.

The behavioral data and fNIRS measurements for all subjects were collected to explore the differences in PFC activity between verbal and spatial memory. To note, the measurements for verbal memory and spatial memory are extracted by subtracting control measurements from their respective noncontrol measurements.

Figure 7 shows that the response time for verbal recognition is higher (about 11%) than spatial recognition ($F(1, 4) = 212, p < 0.001$). The results show that the response time for verbal memory is smaller than that for spatial memory. A possible explanation is that: the circle and inside dot in the spatial control might be considered as a novel mark which may cause subjects' attention and thus reduces the response time, and thus overestimates the response time for spatial memory.

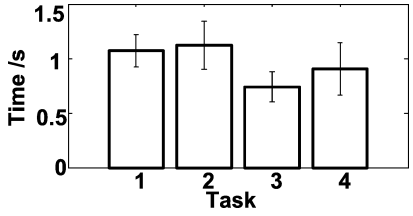

Fig. 7. Response time of verbal control (1), verbal recognition (2), spatial control (3), and spatial recognition (4) in the stem recognition task.

J. Innov. Opt. Health Sci. 2009.02:423-430. Downloaded from www.worldscientific.com
by HUAZHONG UNIVERSITY OF SCIENCE AND TECHNOLOGY on 10/24/18. Re-use and distribution is strictly not permitted, except for Open Access articles.

The fNIRS-measured hemodynamic response during the experiment is similar among subjects. Figure 8 shows the time course of the hemodynamic response for subject 1. The first and second measurement segments with gray background correspond to verbal control and spatial control, respectively. Accordingly, the first and second measurement segments with white background correspond to verbal recognition and spatial recognition. In most channels, Δ[oxy-Hb] shows distinct difference in activation level among the four tasks. Δ[deoxy-Hb] shows lower amplitude of activation than Δ[oxy-Hb] and thus it does not significantly differentiate the activation pattern among the above tasks. The oxygenation, which can be observed as the distance between Δ[oxy-Hb] and Δ[deoxy-Hb] in Fig. 8, shows a clear higher response of verbal recognition than spatial recognition in most channels.

The mean oxygenation changes for verbal memory and spatial memory are extracted to compare the PFC activation between the two functions for each subject. Figure 9 displays the mean comparison across subjects. As shown in Fig. 9, the oxygenation for verbal memory is notably higher than that for spatial memory ($F(1,15) = 72.687, p < 0.001$). Especially, the left PFC shows a much stronger oxygenation change for verbal memory than that for spatial memory. This result agrees with the reported left-lateralization for verbal memory in PET and fMRI studies.[16,17] The oxygenation for spatial memory mainly increased in the middle and right PFC, which is consistent with the research performed by PET.[21–23]

Apart from repeating the activation lateralization for the functions of verbal memory and spatial memory, further, our result provides the comparison on the two functions in PFC activation and the possible relationship among the two functions for Chinese participants. In Fig. 9, bars for verbal

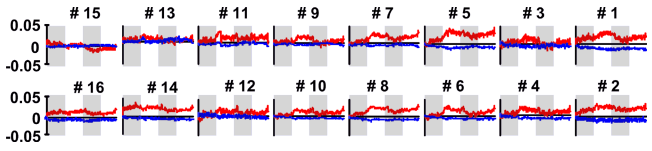

Fig. 8. Time courses of Δ[oxy-Hb] (red line) and Δ[deoxy-Hb] (blue line) obtained by fNIRS in some subjects during the task of stem recognition. The gray regions denote the measurements for verbal control and spatial control in turn; the other regions denote the measurements for verbal recognition and spatial recognition in turn.

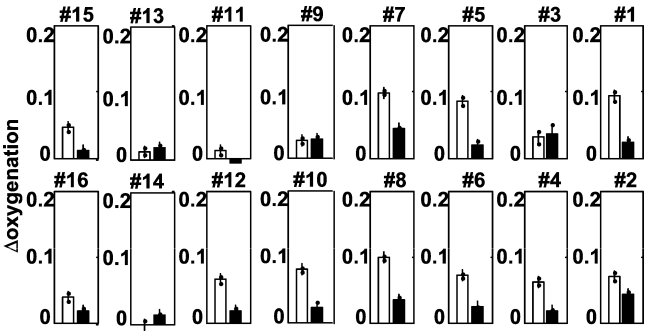

Fig. 9. Mean oxygenation changes of verbal memory (white bar) and spatial memory (black bar) in PFC.

memory in the right PFC indicate that the pure verbal memory also activates the right PFC and the activation of this region is stronger than pure spatial memory. The right PFC is also shown to be a dominant area for verbal memory, although it is not as significant as the left PFC. Considering a previous study showing different activation areas between groups in mother language and non-mother language,[24] a possible reason to the right PFC's dominant activation may be that English is not our mother language. This result indicates that the verbal memory for Chinese people may employ spatial encoding and spatial-related structure encoding, leading to invoking the predominant area for spatial memory.

The measurements on response time and PFC hemodynamic response show some consistency. One common aspect they both exhibit is that the response for verbal control is lower than verbal recognition and the response for spatial control is lower than spatial recognition (see Figs. 7 and 8). The other is that, they both show that the response for verbal recognition is higher than spatial recognition (see Figs. 7 and 8).

4. Conclusion and Discussion

The fNIRS technology has been highlighted as a tool to measure cortical hemodynamic changes in response to functional activities. More pointedly, our fNIRS instrumentation allows for safe, portable, low-cost cortical monitoring and hence can be in real-life situation applied in research and clinical diagnosis. Here, we provided an overview of working memory studies carried out in our laboratory. These studies show that working memory, which is involved in Chinese words encoding, verbal and spatial stem recognition, can be well assessed by

J. Innov. Opt. Health Sci. 2009.02:423-430. Downloaded from www.worldscientific.com
by HUAZHONG UNIVERSITY OF SCIENCE AND TECHNOLOGY on 10/24/18. Re-use and distribution is strictly not permitted, except for Open Access articles.

fNIRS technology. In all above working memory studies, the fNIRS-measured activation patterns are in agreement with the results obtained by the current widely-used PET and fMRI technologies. Our studies suggest that fNIRS would be a promising alternative to the current high cost, invasive, and ionizing methodologies for the studies of functional activities. In addition, the successful assessment of multi-kinds of working memory in free active state indicates that fNIRS has the potential usage for child ability assessment and thus would be beneficial for child development.

Our fNIRS measurements show that PFC indeed activates underlying multi-type working memory, including verbal memory, spatial memory, structure cognition, and semantic processing in Chinese word encoding. The presented study, by conducting multiple experiments and detecting bilateral PFC activation with fNIRS, provides fully evidences in the viewpoint of nontraditional technology to support the involvement of PFC in working memory.

Except for replication, supplement, and specification on the reported findings on the feature of PFC activation, we further find that the fNIRS-measured PFC hemodynamic responses are associated with subjects' behavioral data. For Chinese word encoding, the mean oxygenation and time courses of both Δ[oxy-Hb] and Δ[deoxy-Hb] replicate the polarity between structure cognition and semantic processing in the self-feeling difficulty score. The correlation between mean oxygenation in PFC and self-feeling difficulty scores (difficulty score) for all subjects is quite significant ($r = 0.958, p < 0.001$). For stem recognition, the activation level in time courses of Δ[oxy-Hb] replicate the order of response time among the tasks of verbal control, verbal recognition, spatial control, and spatial recognition; the mean oxygenation in some activated PFC region replicates the polarity in response time between verbal memory and spatial memory.

It is noteworthy that fNIRS measures multiparameters, including Δ[oxy-Hb], Δ[deoxy-Hb], oxygenation, and blood volume (equal to Δ[oxy-Hb] + Δ[deoxy-Hb]), which can provide more information on brain activation and may enable further exploration of the brain functional activities, compared to single parameter for PET, fMRI, and EEG technologies. Take an example, the time courses of Δ[oxy-Hb] and Δ[deoxy-Hb] given in this paper present different signals in response to the brain activity, which may interpret the mechanism of brain function more fully and deeply.

Acknowledgments

We would like to thank all volunteers for their sincere support and effective cooperation in this research. This work has been sponsored by the National Nature Science Foundation of China (Grant no. 30070261, 60025514) and 111 project.

References

1. F. F. Jobsis, "Noninvasive, infrared monitoring of cerebral and myocardial oxygen sufficiency and circulatory parameters," *Science* **198**, 1264–1267 (1977).
2. Y. Hoshi, "Functional near-infrared spectroscopy: Current status and future prospects," *J. Biomed. Opt.* **12**, 062106 (2007).
3. T. Shiga, K. Tanabe, Y. Nakase, T. Shida, B. Chance, "Development of a portable tissue oximeter using near infra-red spectroscopy," *Med. Biol. Eng. Comput.* **33**, 622–626 (1995).
4. S. R. Fanning, S. Short, K. Cole, S. Andresen, H. Moore, G. T. Budd, D. Weng, "Dynamic infrared imaging — a real-time, non-invasive tool for monitoring tumor response to neoadjuvant therapy for breast cancer: An update," *Breast Cancer Res. Treat* **100**, S151–S152 (2006).
5. S. Ke, X. X. Wen, M. Gurfinkel, C. Charnsangavej, S. Wallace, E. M. Sevick-Muraca, C. Li, "Near-infrared optical imaging of epidermal growth factor receptor in breast cancer xenografts," *Cancer Res.* **63**, 7870–7875 (2003).
6. M. Ferrari, L. Mottola, V. Quaresima, "Principles, techniques, and limitations of near infrared spectroscopy," *Can. J. Appl. Physiol.* **29**, 463–487 (2004).
7. Y. Hoshi, "Functional near-infrared optical imaging: Utility and limitations in human brain mapping," *Psychophysiology* **40**, 511–520 (2003).
8. A. Villringer, B. Chance, "Non-invasive optical spectroscopy and imaging of human brain function," *Trends. Neurosci.* **20**, 435–442 (1997).
9. S. C. Bruce, A. Devaraj, M. Izzetoglu, B. Onaral, K. Pourrezaei, "Detecting deception in the brain: A functional near-infrared spectroscopy study of neural correlates of intentional deception," *Proc. SPIE* **5769**, S24–S32 (2005).
10. H. Ogata, T. Mukai, T. Yagi, "A study on the frontal cortex in cognitive tasks using near-infrared spectroscopy," *Conf. Proc. IEEE Eng. Med. Biol. Soc.* **2007**, 4731–4734 (2007).
11. J. Lee, B. S. Folley, J. Gore, S. Park, "Origins of spatial working memory deficits in schizophrenia: An

event-related fMRI and near-infrared spectroscopy study," *PLoS ONE* **3**, e1760 (2008).
12. T. Schreppel, J. Egetemeir, M. Schecklmann, M. M. Plichta, P. Pauli, H. Ellgring, A. J. Fallgatter, M. J. Herrmann, "Activation of the prefrontal cortex in working memory and interference resolution processes assessed with near-infrared spectroscopy," *Neuropsychobiology* **57**, 188–193 (2008).
13. M. Izzetoglu, K. Izzetoglu, S. Bunce, H. Ayaz, A. Devaraj, B. Onaral, K. Pourrezaei, "Functional near-infrared neuroimaging," *IEEE Trans. Neural Syst. Rehabil. Eng.* **13**, 153–159 (2005).
14. A. M. Owen, "The functional organization of working memory processes within human lateral frontal cortex: The contribution of functional neuroimaging," *Eur. J. Neurosci.* **9**, 1329–1339 (1997).
15. E. E. Smith, J. Jonides, "Working memory: A view from neuroimaging," *Cognit. Psychol.* **33**, 5–42 (1997).
16. E. E. Smith, J. Jonides, "Storage and executive processes in the frontal lobes," *Science* **283**, 1657–1661 (1999).
17. T. S. Braver, J. D. Cohen, L. E. Nystrom, J. Jonides, E. E. Smith, D. C. Noll, "A parametric study of prefrontal cortex involvement in human working memory," *Neuroimage* **5**, 49–62 (1997).
18. Y. Zheng, Z. Zhang, Q. Liu, C. Cao, H. Gong, "Design and evaluation of a portable continuous-wave NIR topography instrument," *Proc. SPIE* **6047**, 60470X (2006).
19. H. Obrig, A. Villringer, "Beyond the visible-imaging the human brain with light," *J. Cereb. Blood Flow Metab.* **23**, 1–18 (2003).
20. M. J. Herrmann, M. M. Plichta, A. C. Ehlis, A. J. Fallgatter, "Optical topography during a Go-NoGo task assessed with multi-channel near-infrared spectroscopy," *Behav. Brain Res.* **160**, 135–140 (2005).
21. E. E. Smith, J. Jonides, R. A. Koeppe, "Dissociating verbal and spatial working memory using PET," *Cereb. Cortex* **6**, 11–20 (1996).
22. E. E. Smith, J. Jonides, R. A. Koeppe, E. Awh, E. H. Schumacher, S. Minoshima, "Spatial vs. object working memory: PET investigations," *J. Cognit. Neurosci.* **7**, S337–S356 (1995).
23. J. Jonides, E. E. Smith, R. A. Koeppe, E. Awh, S. Minoshima, M. A. Mintun, "Spatial working memory in humans as revealed by PET," *Nature* **363**, 623–625 (1993).
24. C. Pallier, S. Dehaene, J. B. Poline, A. M. Argenti, E. Dupoux, J. Mehler, "Brain imaging of language plasticity in adopted adults: Can a second language replace the first?," *Cereb. Cortex* **2**, S155–S161 (2003).
25. S. Zeng, J. Yang, L. Guan, P. Kuang, H. Gong, B. Chance, "Observing prefrontal activation during semantic encoding with near infrared diffusive imaging," *Acta Photonica Sinica* **29**, 1–3 (2000).
26. J. Yang, S. Zeng, Q. Luo, L. Guan, P. Kuang, H. Gong, W. Lichty, B. Chance, "Hemispheric asymmetry for encoding unrelated word pairs? A functional near-infrared spectroscopy study," *Space Med. Med. Eng.* **18**, 318–323 (2005).

J. Innov. Opt. Health Sci. 2009.02:423-430. Downloaded from www.worldscientific.com
by HUAZHONG UNIVERSITY OF SCIENCE AND TECHNOLOGY on 10/24/18. Re-use and distribution is strictly not permitted, except for Open Access articles.